Stony Brook University

Crystallization kinetics and crystal morphology of ultrathin polycaprolactone films directed by supercritical carbon dioxide.

A thesis presented

by

Mani Kuntal Sen

to

The Graduate School

in partial fulfillment of the

requirements

for the degree of

Master of Science

in

Materials Science and Engineering

Stony Brook University

August 2012

Stony Brook University

The Graduate School

Mani Kuntal Sen

We, the thesis committee for the above candidate for the

Master of Science degree, hereby recommend

acceptance of this thesis.

Dr. Tadanori Koga – Dissertation Advisor
Assistant Professor, Materials Science and Engineering

Dr. T. A. Venkatesh
Assistant Professor, Materials Science and Engineering

Dr. Dilip Gersappe
Associate Professor, Materials Science and Engineering

This thesis is accepted by the Graduate School

Charles Taber
Interim Dean of the Graduate School

Abstract of the Thesis

Crystallization kinetics and crystal morphology of ultrathin polycaprolactone films directed by supercritical carbon dioxide.

By

Mani Kuntal Sen

Master of Science

In

Material Science and Engineering

Stony Brook University

2012

The effects of supercritical carbon dioxide ($scCO_2$) as an effective plasticization agent on the crystallization kinetics and crystal morphology of ultrathin polycaprolactone (PCL) films (less than 100nm in thickness) were studied by using various techniques including optical microscopy, atomic force microscopy, and x-ray scattering experiments. As a result, it is found that the PCL chains form "flat-on" lamellae, where the lamellar layers run parallel to the substrate surface, irrespective of the CO_2 process conditions and the film thickness. It was also found that the unique $scCO_2$ conditions near the critical point (critical temperature (Tc) =31.3°C and critical pressure (P_C) =7.38MPa) result in the significant enhancement of the crystal size compared to those under the other $scCO_2$ process conditions or conventional high-temperature annealing process. Furthermore, it was found that $scCO_2$ induces the secondary heterogeneous nucleation of the excess melt on the film surface during the isothermal re-crystallization process.

Table of Contents

List of figures:

Acknowledgements

The journey through my Masters degree has been very challenging as well as memorable time of my life and it would not have been possible without a considerable amount of help and support from the people around me.

First I would like to thank my guide and mentor, Prof. Tadanori Koga for giving me this wonderful opportunity. His academic guidance, inspiration and undying support have been invaluable to me. This work would not have been possible without his encouragement and patience.

Furthermore, I would like to thank my lab mates Naisheng Jiang and Peter Gin for our long and fruitful discussions on various topics and I appreciate their help and advice. I would also like thank the beam line scientist at Brookhaven National Laboratory, Steve Bennett who helped me with the x-ray scattering experiments.

Finally I would like to thank my committee members Prof. T. A. Venkatesh and Prof. Dilip Gersappe for their support and time. I would also like to thank my fellow friends at Stony Brook University for their inspiration and constant support.

Crystallization kinetics and crystal morphology of spin coated polycaprolactone films on silicon substrate processed by conventional annealing and supercritical carbon dioxide.

Chapter 1: Introduction:

1.1: Polycaprolactone:

Polycaprolactone (PCL) $(C_6H_{10}O_2)_n$ is one of the most commonly used biodegradable polymers [1]. It is produced from crude oil. It has a good resistance to water, oil and chlorine. It is a hydrophobic, semi-crystalline polymer having a glass transition temperature (Tg) of −60 °C (approx.) and a low melting point of 54˚C-64˚C [2]. It is currently used in the following major applications:

1) Making super specialty polyurethanes.
2) Used in preparation of long term implantable devices because of slower degradation of polymer.
3) Used in drug delivery in the human body.

1.2: Thin and ultrathin polymer films:

Polymer films are mainly classified on the basis of film thickness. Typically films of thickness less than 100nm are called ultrathin films and films of thickness above 100nm to the order of few microns are called thin films. Polymer thin and ultrathin films have various real life applications in the fields of molecular electronics, optics, sensors and solar cells. Recently polymer crystallization in thin (100nm- few microns) and ultrathin films (thickness less than 100nm) on solid substrates have attracted increased attention because of the fact that crystalline morphology and crystal growth of thin and ultrathin polymer films are quite different from bulk [3]. Two major reasons to study the crystallization of polymer in thin and ultrathin films are: (i) to develop new technologies and to enhance device performance, (ii) to elucidate the fundamental issues of polymer crystallization in general. Moreover a polymer thin film can be considered as a one- dimensional (1D) confinement system where the effects of confinement and interface are profound than bulk.

1.3: Polymer crystallization on films:

The process of polymer crystallization is a transition from a randomly coiled state to a perfectly ordered state. During this process a hierarchy of ordered structure develops which in turn controls the physical properties of the polymer materials. In bulk, spherulites are the most common superstructures observed when crystallized from melt, while single crystals and dendrites can be crystallized from dilute solutions [4]. The concept of folded-chain crystal [fig. 1] formed during crystallization in polymer films from melt has been widely accepted. The crystalline structures with one dimension of only several nanometers, which are known as lamellae are the basic building blocks of the crystalline polymer substances. However chain folded crystals are non-equilibrium structures that are trapped in metastable states with a significant degree of disorder characterized by the degree of chain folding [5]. In recent years there has been a common understanding that the structure of the polymer crystals is governed by kinetic factors [6] which is related to degree of supercooling, film thickness, segmental mobility and surface free energy at the interface. It is also generally believed that film thickness that characterizes the degree of confinement together with strength of substrate-polymer interface interaction and degree of super cooling are the most important parameters in thin film system for crystallization. Moreover the resulting crystal growth rate is a function of the lamellar thickness. Despite all these studies, comprehensive insights in polymer crystallization have not been obtained especially in case of thin and ultrathin films.

Fig. 1: Schematic of chain folding mechanism during polymer crystallization [16]

1.4: Crystallization kinetics:

Crystallization kinetics plays an important role in the intermediate and final morphologies formed during and after crystallization in polymer films. Usually the crystallization process consists of two steps: nucleation and crystal growth.

Nucleation can be homogeneous or heterogeneous although homogenous nucleation is rarely seen. Homogeneous nucleation occurs without the formation of any pre-formed nuclei and heterogeneous nucleation occurs with the introduction of foreign surfaces. Following the nucleation process, nuclei continue to grow by adding new amorphous materials to the existing crystal growth front, resulting in various macroscopic crystal patterns ranging from geometrical-simple single crystals to highly complex superstructures like spherulites. A general trend in the crystallization kinetics where the rate of crystallization decreases significantly with decrease of film thickness is reported in literature. Three possible explanations for the slowing down in crystallization kinetics are provided till date: a reduction of molecular mobility due to increase in the glass transition temperature of the polymer [7, 8], the presence of a reduced mobility layer at the polymer/substrate interface [9, 10], and the reduction of the number of active nuclei as thickness decreases [11, 12].

1.5: Crystal structure and morphology:

Despite the presence of confinement and the substrate effects, semicrystalline polymers can crystallize in a conventional manner whereby polymer chains fold back and forth into stems to form lamellae. One of the greatest differences between polymer lamellae and small molecule single crystals is the anisotropy of their surface structures. As shown in Fig. 2, polymer lamellae are bounded by two basal surfaces covered by chain folds and several lateral surfaces. Although the exact structure of the fold surface, which may differ according to how the lamellae are formed, is not clear at present [13], it is believed that chain folds are mainly in amorphous or quasi-amorphous state in contrast to the lateral surface of polymer lamellae and the fully crystallized faces of small molecule single crystals. Therefore, the surface energy of the fold surface is quite different from that of the lateral surface: the former is generally ten times larger than the latter, which is much stronger than the differences among different crystalline faces of small molecule single crystals. In bulk, the anisotropic lamellae can isotropically distribute. However, for the thin films with thickness reduced to the lamellar thickness or to small multiples of it, the anisotropic surface properties will eventually take effect because lamellae cannot rotate freely in 1D confinement space. As a result, preferential lamellae orientations are produced in thin and ultrathin films. Indeed, the preference of lamellar orientations is widely confirmed by experiments and has emerged as one of the major areas in crystallization of polymer films.

Generally, two preferred orientations are encountered mostly in experiments: perpendicular (edge-on lamellae) and at the other extreme parallel (flat-on lamellae) to the substrate surface.

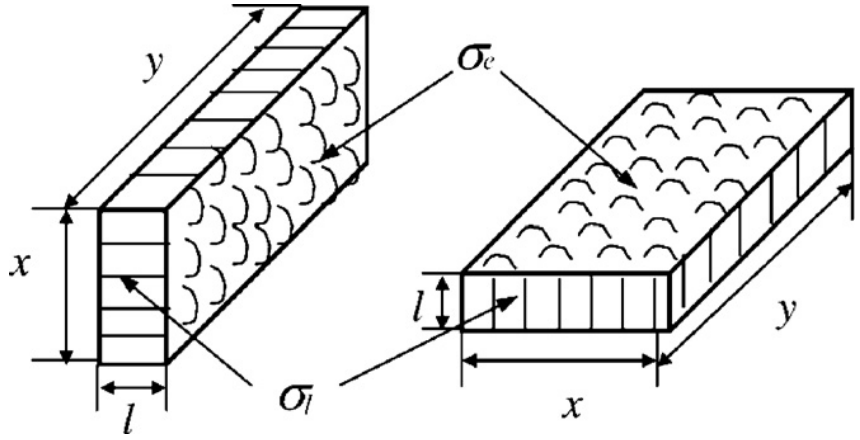

Fig 2: Schematic of edge-on lamellae (left) and flat-on lamellae (right). Substrate backbone is parallel in case of edge-on lamellae and perpendicular in case of flat-on lamellae. Lamellar thickness is denoted by l and the two other dimensions are denoted by x and y respectively. Fold surface energy (σ_e) is much larger than the lateral free energy (σ_l) [4]

Edge on lamellae are usually in fibrous form with nearly uniform width, which aggregate further into axialites, hedrites, and spherulites, whereas flat-on lamellae may exhibit complicated patterns (dendrites, seaweeds) as well as regular forms (hexagons, squares, and lozenges) of faceted single crystals. Various techniques, including transmission electron microscopy (TEM) and electron diffraction (ED), scanning electron microscopy (SEM), atomic force microscopy (AFM), optical and polarized optical microscopy (OM and POM), grazing incidence wide angle X-ray diffraction (GIWAXD) and grazing incidence small-angle X-ray scattering (GISAXS), reflection high energy electron diffraction (RHEED), grazing incidence reflection absorption Fourier transform infrared spectroscopy (RA-FTIR), and dielectric spectroscopy (DS), have been employed to study the crystallization of polymer ultrathin films on solid substrates for last two decades. In most cases, by using imaging methods such as AFM, TEM, and OM, lamellar orientation can be easily recognized through morphology. Typical images of edge-on and flat-on lamellae are shown in fig. 3.

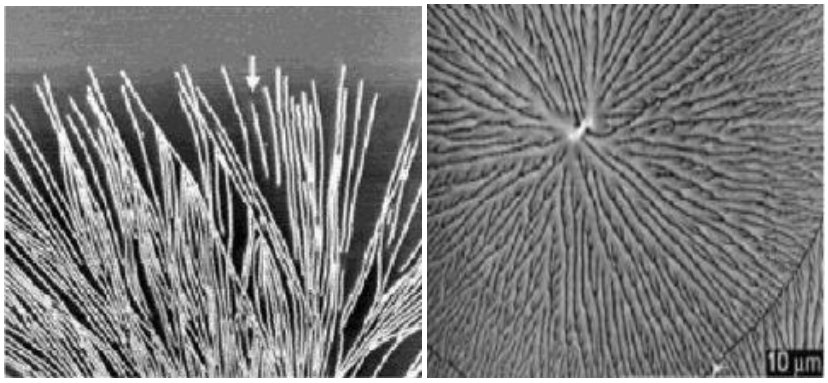

Fig. 3: Edge-on lamellae (left) [14] and flat-on lamellae (right) [15]

1.6: Literature Review:

A variety of properties of thin film materials depend significantly on the free surface and buried interface [17, 18]. Understanding the effects of surface and interface on the structural aspects of thin films is essential to many applications and has led to an increasing interest in thin film behavior at free surface and buried interface. Because of the fact that more than two-thirds of the synthetic polymers are semi crystalline materials, studies on the crystallization behavior of thin and ultrathin polymer films on foreign surfaces are of great importance. In general, edge-on lamellae with the highest nucleation rates have been predicted to predominantly form at a free surface at low temperatures [19-22]. In contrast, flat-on lamellae with the highest heterogeneous nucleation rates form at polymer-substrate interfaces at high temperatures [23, 24]. The effects of the free surface and the buried interface are thus in a competing relationship in thin film crystallization of polymers. For thicker films, the effect of the free surface plays a leading role, which results in the formation of edge-on lamellar crystals as the predominant morphology [25-28]. For ultrathin films with thicknesses close to that of polymer coil sizes, the effects of the buried interface generally control the nucleation and result in polymers growing predominantly into flat-on lamellar crystals [29-40]. Qiao et al. [41] have studied the confinement effects on the crystallization behaviors of PCL in thin and ultrathin films. It is reported that for film thickness less than 100nm, spherulitic structure can be formed due to nucleation process. It is also believed that 2Rg (radius of gyration) is the critical thickness for PCL crystallization to differ from bulk behavior. PCL ultrathin films have been reported to crystallize with lamellae orientated flat on when crystallized at room temperature on a hot stage (in-situ), where the morphologies are dendritic in nature for thinner films (thickness≤15nm), and flat-on axialites covered by many

overgrowths for thicker films (thickness≥30nm) with some branched edge-on lamellae observed in film thickness of 120nm and 200nm [42].

1.7: Research motivation and objectives:

As discussed above, despite extensive studies on polymer crystallization, comprehensive insights has not been obtained completely yet, especially for polymer crystallization in semicrystalline polymers in thin and ultrathin films. Moreover the effects of free surface and buried surface on polymer crystallization have not been understood properly. There are some other factors like the rate of supercooling and confinement which can also have a profound effect on the morphology of crystals in polymer crystallization. Crystal morphology can greatly influence the mechanical and optical properties of any crystalline material [43, 44]. In this thesis, an effort has been made to study the crystallization behavior of PCL and thereby understand and shed some light into the crystallization kinetics of PCL (a model semicrystalline polymer) under the effects of different degrees of supercooling together with confinement effects and the role of different interfaces in the process of crystallization. We also use supercritical carbon dioxide ($scCO_2$) as a plasticizer in addition to conventional annealing process to control the morphology and crystallization PCL thin and ultrathin films. The research goal is to compare the crystallization process and kinetics in PCL films due to exposure to $scCO_2$ and the effect of $scCO_2$ on the crystallization behavior of PCL films compared to conventional annealing process. Lamellar orientation of the crystals on substrate due to effects of supercooling and confinement has also been studied.

PCL was chosen for its biodegradable properties which are required in the field of drug delivery [45] and tissue engineering [46]. Moreover a low melting point, close to 60˚C like PEO, but with much more lower growth rates (around 500 times less at 46˚C for example) [47, 48], make PCL a convenient polymer for practical reasons. Finally PCL can be considered as an alternative model for study of polymer crystallization, with a crystal structure very close to that of polyethylene (PE) [49], the "model" semicrystalline polymer. Moreover our group has also reported the supercritical carbon dioxide induced surface melting/recrystallization process in ultrathin PEO films. Hence this thesis work is a good opportunity to compare polymer crystallization in two different semicrystalline polymer systems (PEO and PCL) and hopefully understand fundamental issues of polymer crystallization in semicrystalline polymers.

Chapter 2: Materials and Methods

2.1: Preparation of polymer solutions:

Solutions for PCL (average M_n= 45,000, Sigma Aldrich) films (20-50-100-200nm) were prepared using varying concentrations of PCL from 0.79%, 1.2%, 2.6%, and 8% in toluene (99.5%, Sigma Aldrich). The solutions were heated at 60˚C on a hot stage for 15 minutes to dissolve the polymer completely in toluene.

2.2: Cleaning of silicon wafers:

Silicon (Si) wafers are chosen as a substrate for PCL films. Si wafers (1 0 0) were cut into small pieces of size 2cm x 2cm. They were put in a beaker and washed 5 times with distilled water to remove any broken Si particles or other foreign particles. Then 50ml of distilled water, 50 ml of hydrogen peroxide (Fisher Chemical, H325-500) and 50ml of ammonia solution (Avantor Performance Materials, 10-30% ammonia) were taken in a beaker together with the Si wafers and heated at 150˚C for 20 minutes. The same step was performed again but with 50ml of sulfuric acid in place of ammonia solution. The wafers were washed with distilled water after draining the waste solution for 5 times in between the two steps and after the final step.

2.3: Preparation of PCL thin and ultrathin films:

PCL films were prepared using spin coating technique. An in-house spin coater (Headway Research Inc., Texas) was used to prepare the films. Before spin casting, the native oxide layer on Si wafers was removed by dipping the wafers in a diluted solution of hydrochloric acid (Sigma-Aldrich) for 15 sec. Subsequently, the polymer solutions were pipetted onto the cleaned Si wafers until completely wet and spun-cast with a rotation speed of 2500 rpm for 30 s. Uniformity of the spun-cast films were evaluated using both standard spectroscopic ellipsometry and x-ray reflectivity.

2.4: Measuring the thickness of the films:

An ellipsometer (Rudolph Research) was used to measure the thickness of the polymer films. Ellipsometry is a technique based on measurement of the change of the polarization of light after reflected on or transmitted through the samples. During the measurement, a laser beam is used as the light source, and the light emitted by the laser is polarized by a polarizer and it hits the

surface of the sample. After reflection, the reflected light passes though a compensator and a second polarizer and finally goes to a detector [50-52]. Fig. 4 is a schematic diagram of the principle of ellipsometry. In this experiment, the refractive index for PCL has been taken as 1.476 for thickness measurement purposes.

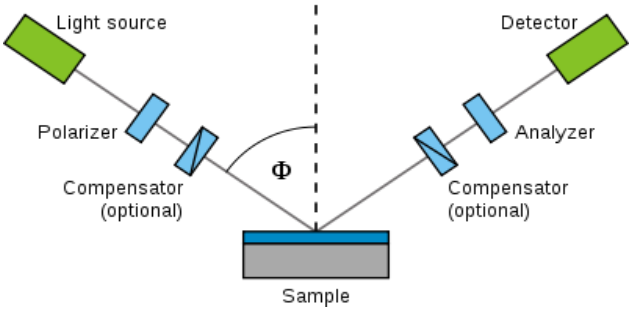

Figure 4. Schematic diagram of ellipsometry [53]

2.5: Thermal annealing and super critical carbon dioxide ($scCO_2$) exposure:

To drive the recrystallization process in the polymer films, the samples were either thermally annealed or exposed to $scCO_2$. Thermal annealing was performed under high vacuum in an oven at 85 °C for 2 h, well above the melting temperature (T_m) of PCL polymer and then the samples have been subjected to recrystallization on a temperature controlled hot stage to various temperatures for 24 hrs in air. Exposure to $scCO_2$ was performed in a custom designed high pressure chamber [Fig. 5] (further details can be found elsewhere [54]). Supercritical carbon dioxide ($scCO_2$) is an environmentally benign solvent, nonflammable and non-toxic. The supercritical condition is achieved at temperatures and pressures above their critical points. Under supercritical conditions, CO_2 has the behavior of both gas and liquid, with very high diffusivity like gas and liquid-like density. The critical temperature for CO_2 is 31.3˚C and critical pressure is 7.38 MPa for supercritical conditions. The temperature of the chamber was regulated and monitored by a water circulator and omega thermocouple respectively. CO_2 was injected from a gas cylinder and pressurized by a pressure generator to ridge condition and the samples were exposed for 2 hours. Rapid drying of the films after exposure was accomplished by quickly venting the gas to the atmosphere in case of quick quench process. Slow venting of the gas to the atmosphere at the rate of decrease of initial pressure by 1psi per second up to ambient pressure was performed during slow quench process. The samples were placed inside a high pressure

chamber (as shown in fig. 5) and pressurized to 10.5 MPa at 50˚C (ridge condition) and kept at that condition for 2 hrs before depressurizing it to ambient pressure either rapidly or slowly (at a rate of decrease of 1 psi per sec. to atm) and keeping the samples inside the chamber at different temperatures of crystallization for 24 hrs.

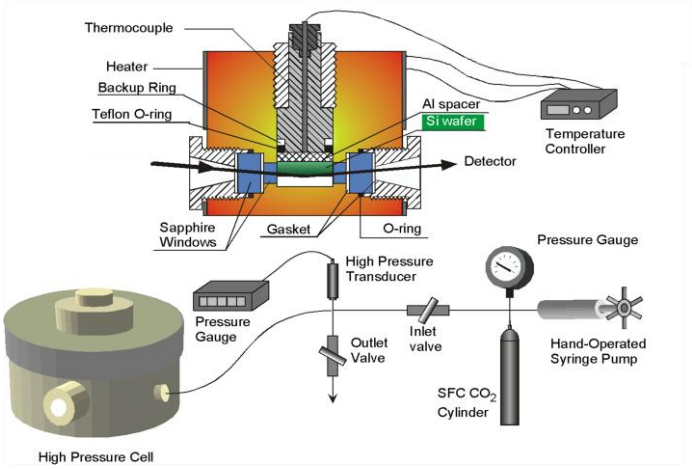

Figure 5: Schematic of a supercritical carbon dioxide chamber

2.6: Obtaining surface information of the films:

The techniques used to evaluate the surface of the processed films to get the information about the morphology and the orientations of the crystals are atomic force microscope (AFM), polarized optical microscope (POM), grazing incidence small angle x-ray scattering (GISAXS) and grazing incidence x-ray diffraction (GIXRD or GID).

Localized surface textures of the films were mapped using contact mode AFM (Digital Instruments, USA). Images were obtained using a Dimension 3000 scanning probe microscope with a Nanoscope controller. Silicon nitride scanning tips (Veeco, NP-10), which vibrates close to its resonance frequency of 75 kHz, were used. The scan rate (optimized for each film) ranged between 0.5-1.0.

Surface morphology was examined using polarized optical microscope (Olympus) equipped with a CCD color camera and the images were analyzed using Image J software.

X-ray scattering experiments were performed at the National Synchrotron Light Source (NSLS) at Brookhaven National Laboratory in Upton, NY. Beam lines X10A and X22B at Brookhaven National Laboratory were used for GID [Fig. 6] experiments with corresponding x-ray energy: 11.3kev and 8.171kev; wavelength of x-rays: 0.1093nm and 0.1517nm; detector pixel size: 0.1mm and 0.115mm and distance from sample to detector: 108.3mm and 203.6nm respectively. The beam in both cases was monochromatized using a Ge(111) crystal and focused onto the sample. The samples to detector distances were calibrated by standard sample of alumina and by standard sample of silver behenate respectively. The samples were mounted in a Kapton chamber to minimize both sample damage and air scattering. The angle of incidence was chosen at 0.2°, and the scattered radiation was collected as a function of the angle 2θ in the film plane at a small exit angle α_f using a scintillation detector. In this way, the intensity was recorded in dependence of the moment transfer $q_{||}$in the surface plane, giving information on the in-plane crystalline structure. The selected incidence angle is much larger than the average critical angle of the polymer film (α_c=0.139°) allowing bulk sensitive GIXRD measurements.

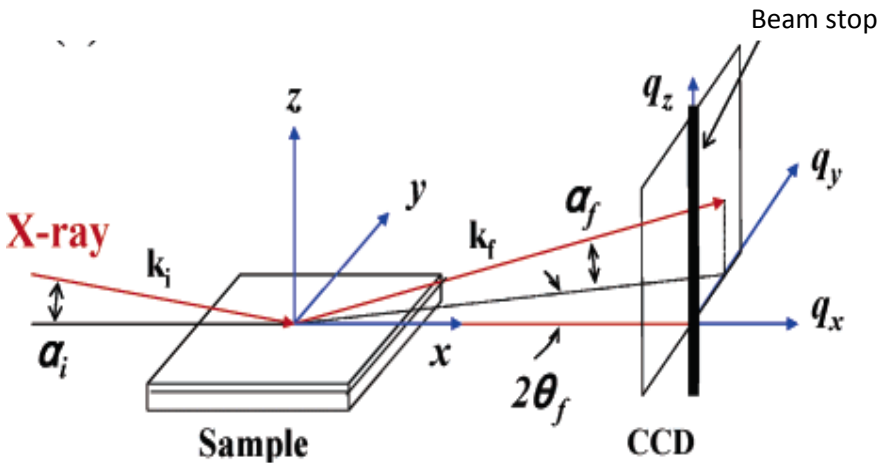

Figure 6: Schematic of GID or GIXRD [55]

Chapter 3: Results and discussion:

3.1: Swelling behavior of PCL ultrathin films in supercritical carbon dioxide:

PCL ultrathin films (100, 50 and 20nm) have been exposed to supercritical carbon dioxide at both 36˚C and 50˚C and corresponding pressures to study the swelling behavior of the polymer during both rapid and slow quench process. Figure 7 shows a plot of linear dilation (linear dilation= $L-L_0/L_0$, where L and L_0 are the swollen and as cast thickness respectively) against the as cast initial thickness (L_0) of the films. With regard to the behavior of CO_2 in the vicinity of its critical point (Tc=31.3 °C and Pc=7.38 MPa), an anomalous maximum is known to occur, which was first observed in the adsorption isotherm of CO2 on carbon black [56] and on silica surfaces [57, 58]. In the present experiments, a deviation from the general behavior can be seen and the anomalous swelling behavior of the polymer is noticed at a higher temperature and pressure which may be explained as lower pressures are not enough to melt the semi crystalline polymer and the sorption of $C0_2$ molecules in the polymer is very limited. Moreover there is a strong enhancement of swelling in thinner films rather than thicker ones as the behavior of anomalous swelling is found to scale with radius of gyration (R_g) of the polymer and the effect extends almost up to $10R_g$ [59]. The R_g for PCL is calculated to be approximately 6nm. The swelling of PCL films is more than other semi crystalline polymers like PEO under the same conditions due to the presence of carbonyl bonds where the electron pair on the PCL carbonyl oxygen interact with the carbon atom of CO_2. Such an interaction explains the unusual swelling of PCL at high-pressure of $scCO_2$. Similar arguments have been reported for PMMA [60]. Unlike the general trend where polymer swelling is more when depressurized rapidly due to "freezing" of the swollen structure compared to a slower depressurization, an opposite behavior is noticed here. This could be explained by considering that, when solvent CO_2 molecule penetrates into the PCL polymer and all accessible free volume is already occupied it has to create a gap of sufficient size to enter and be accommodated in the amorphous matrix. If crystallinity is high (in case of PCL (M_n=45,000), the crystallites also decrease the chain mobility of the rubbery segments, and it is likely that the excess space created by the solvent molecule when penetrating the polymer matrix is not fully recovered, meaning that some sort of new free volume is created by penetration of the solvent molecules when slowly depressurized over a certain time. In this way, a kind of pseudoequilibrium state is established, and the actual equilibrium state cannot be reached, on a reasonably short timescale, due to the presence of rigid crystallites in the polymer matrix.

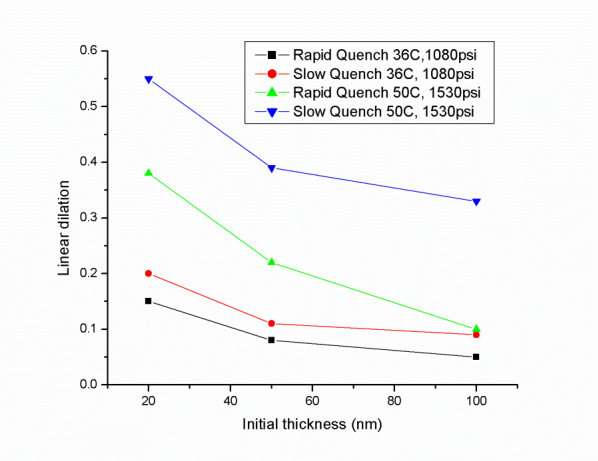

Figure 7: Linear dilation ($L-L_0/L_0$, where L and L_0 are the swollen and as cast thickness respectively) has been plotted as a function of initial thickness of the films exposed to $scCO_2$ at different temperatures and pressures.

3.2: Effect of annealing on morphology and crystallization of PCL thin and ultrathin films

PCL films samples were annealed at 85˚C for 2 hrs under high vacuum and subsequently re-crystallized on a hot stage in air to different Tc (temperature of crystallization) as indicated in figure 8.

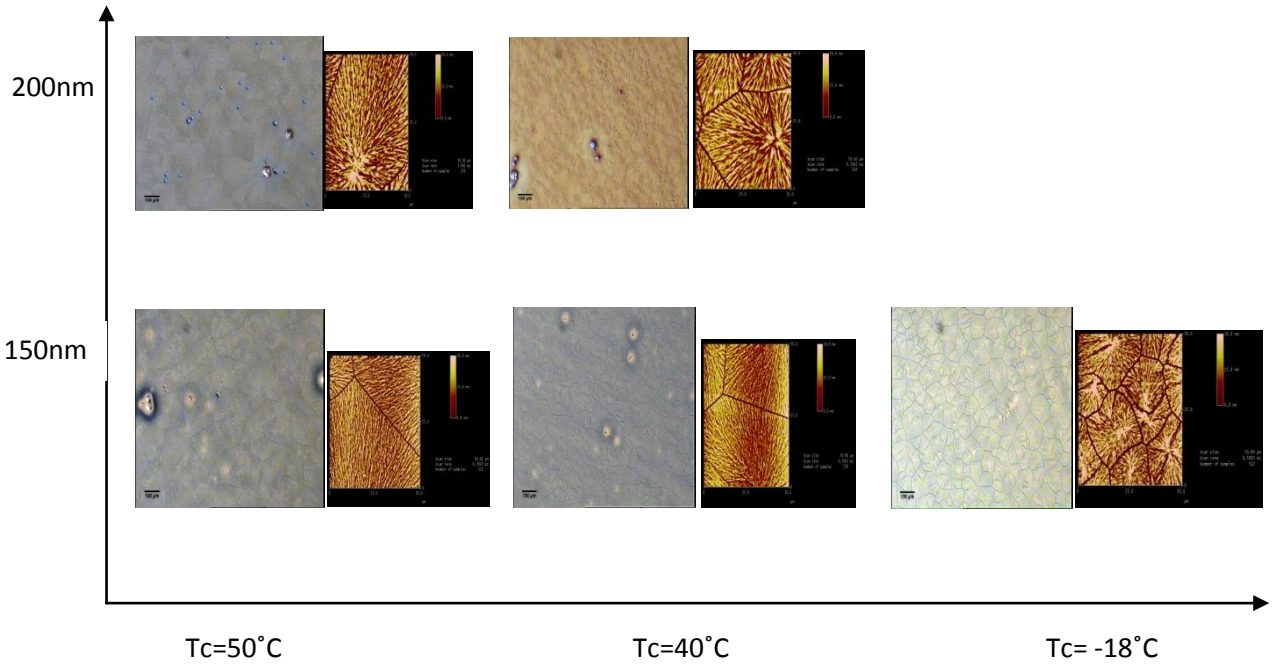

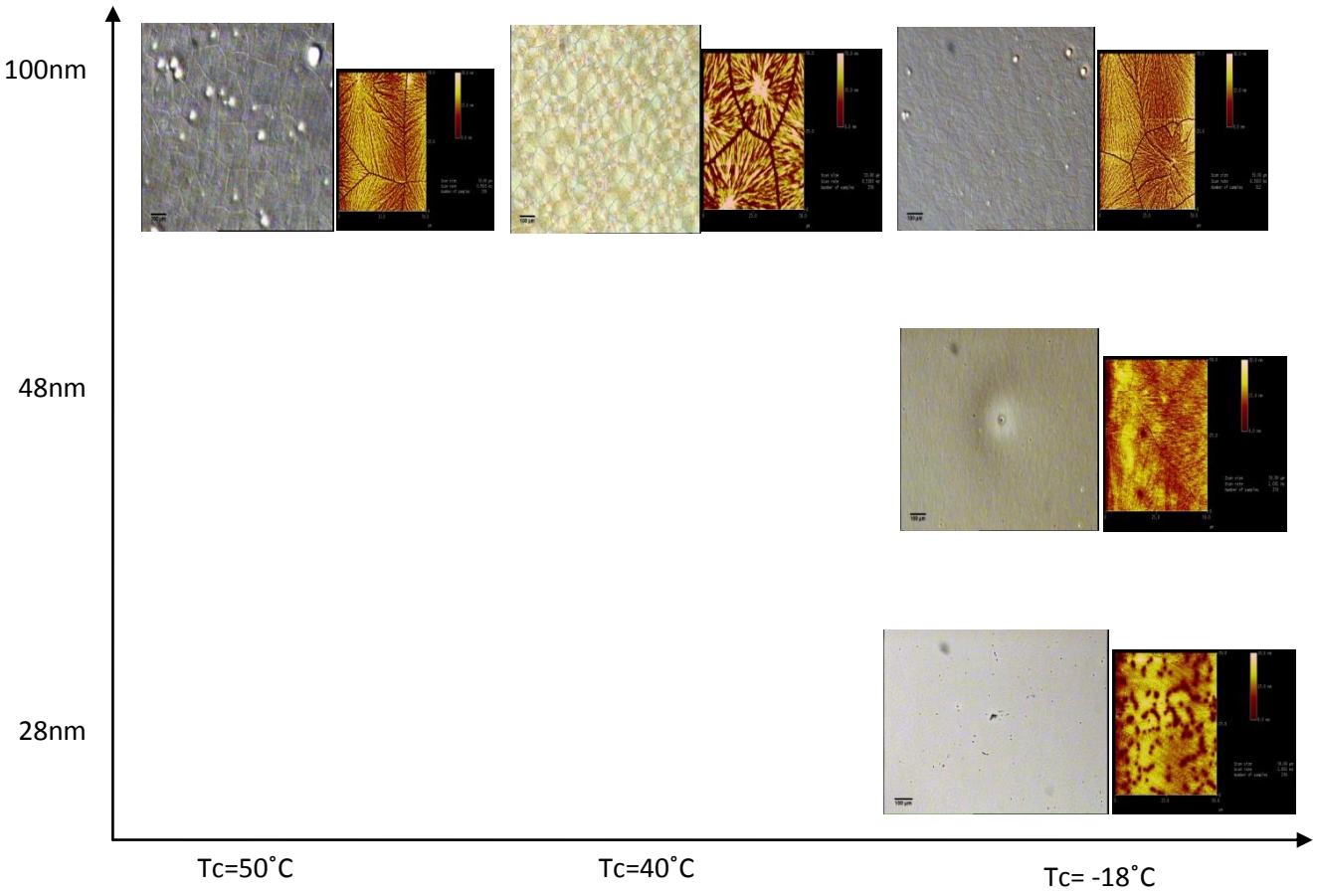

Fig. 8: POM and AFM micrographs of PCL films annealed and re-crystallized at different Tc

The above micrographs show that the surface is covered with several spherulites whose size decreases with the increase in the supercooling. At thickness comparable to 5Rg of the polymer, polymer can no longer form big spherulites and tend to crystallize in small pockets forming a hill-valley structure. Moreover it can be noted that each grain of spherulite has a central nucleating point from which fingers of the lamellae spread in all directions. The shape of the spherulites becomes increasingly random with the increase of degree of supercooling. The temperatures of crystallization were chosen as 50˚C (near the reported melting temperature of aprox. 60˚C), 40˚C (near the onset temperature of crystallization for bulk PCL [61]) and -18˚C (the lowest possible temperature) to study the crystallization behavior over a vast range of temperature and the study the effects of supercooling and confinement on crystallization of the polymer.

3.3: Effect of supercritical carbon dioxide on morphology and crystallization of PCL thin and ultrathin films:

Samples of PCL films were exposed to supercritical carbon dioxide at 10.5 MPa and 50˚C (ridge condition) for two hours, quenched to ambient pressure (rapid and slow) and kept inside the high pressure chamber at different temperatures of crystallization (Tc) for 24 hours. The morphology of the films together with the crystallization behavior was studied using polarized optical microscope (POM) and AFM after taking out the samples from the chamber [Fig. 9].

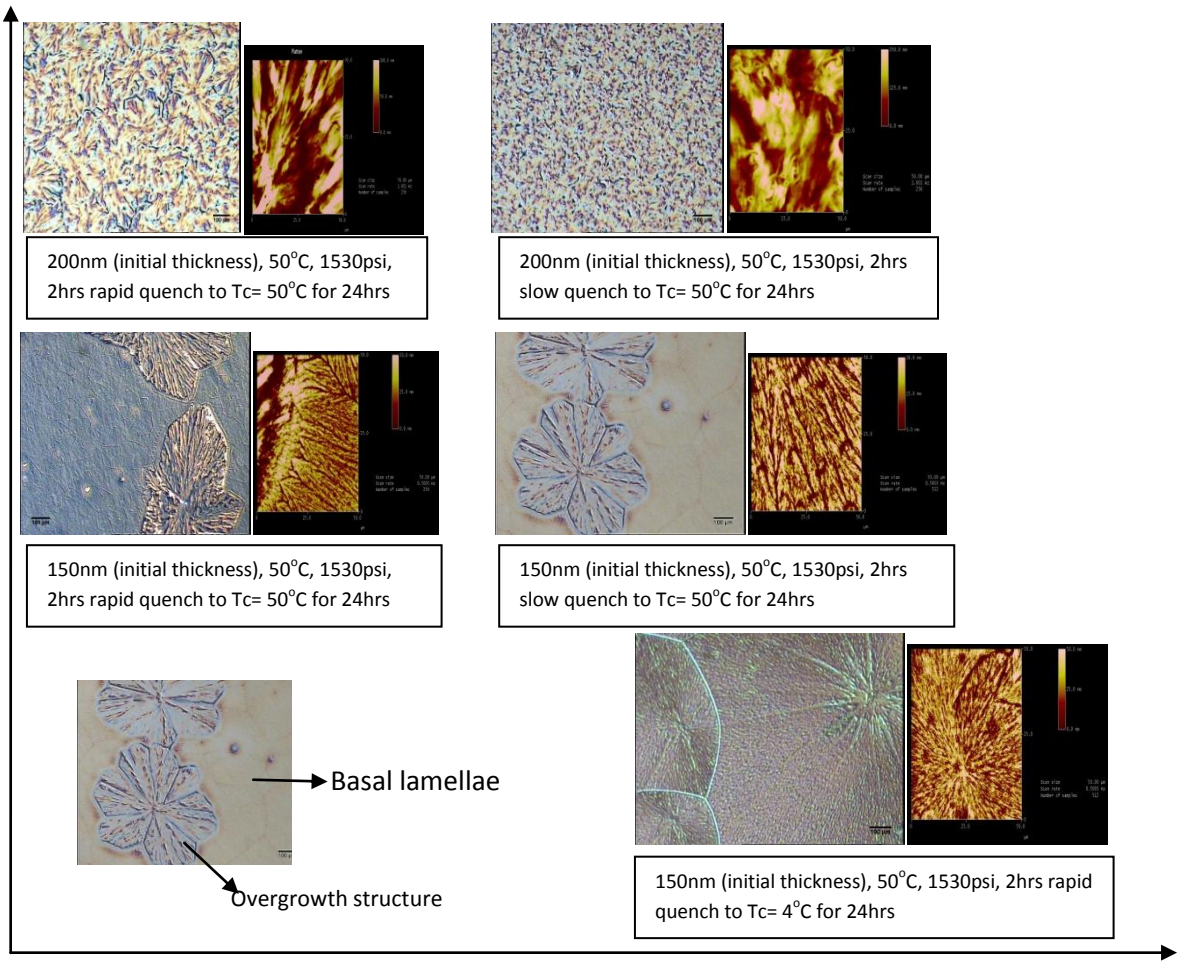

Fig. 9: POM and AFM micrographs of PCL thin films exposed to $scCO_2$ and re-crystallized at different Tc

From the above micrographs, it is clearly observed that overgrowth structures in the shape of multi-faceted petals are formed together with the basal lamellae. It is also noticed that overgrowth structures fail to form in higher super cooled films and subsequent experiments have shown that the overgrowth structures are only noticed if the samples are crystallized at temperatures near T_m (bulk melting temperature) or isothermally.

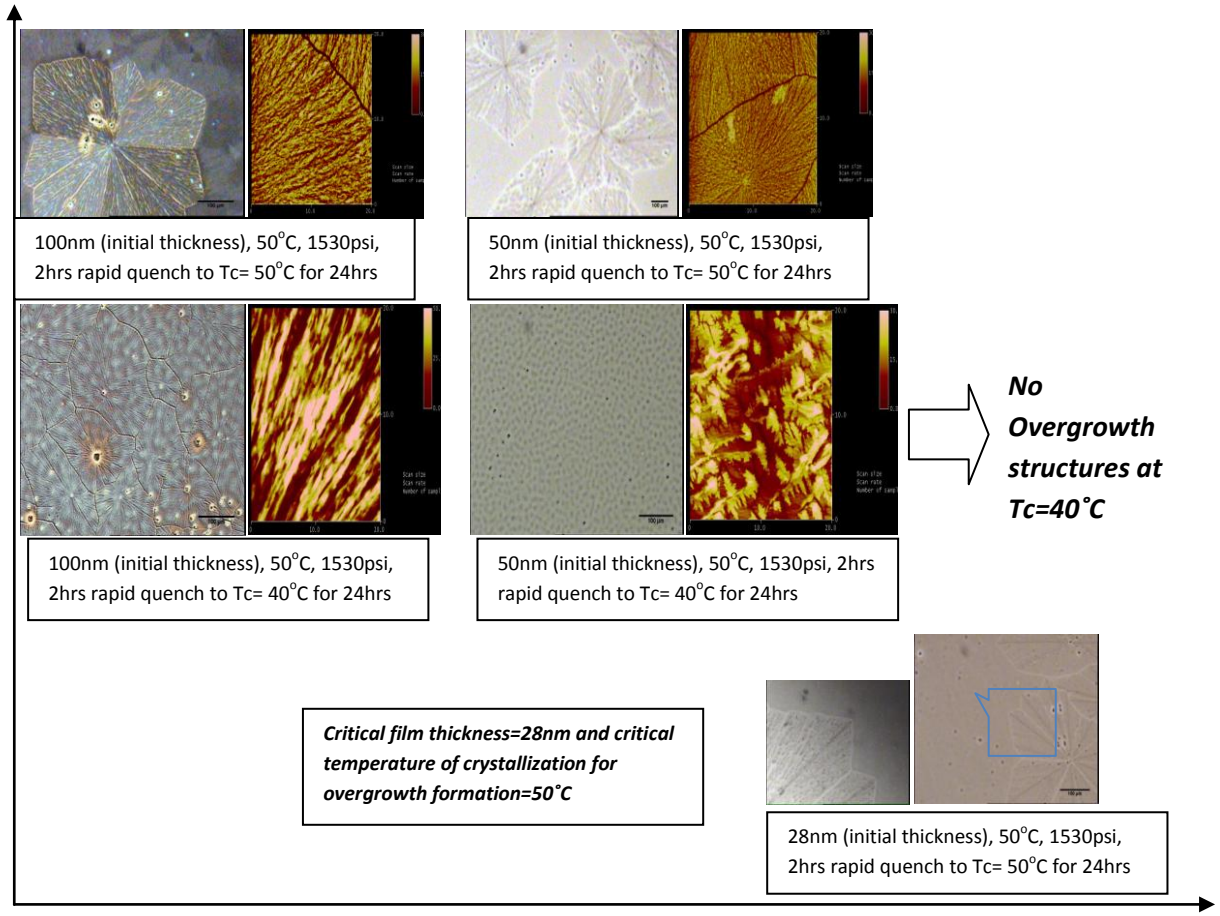

Fig. 10: POM and AFM micrographs of PCL ultrathin films exposed to $scCO_2$ and re-crystallized at different Tc

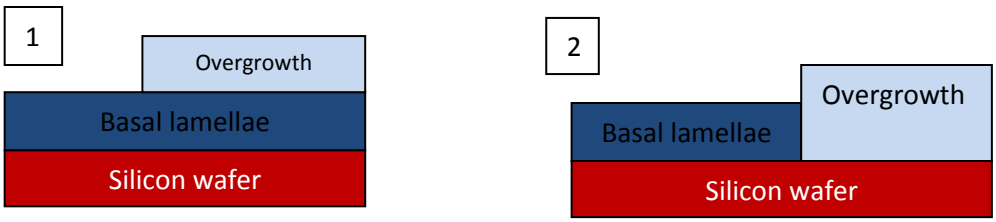

Fig. 11: Two possible arrangements of overgrowth lamellae and basal lamellae on silicon formed during re-crystallization process of PCL after exposure to $scCO_2$

The size of the overgrowth structures decreases with the decrease of film thickness due to the lack of melt during the re-crystallization process. The critical film thickness when there is enough melt for formation of overgrowth lamellae is approximately 5Rg [Fig. 10]. Overgrowth lamellae formation is only observed if the samples are crystallized isothermally. The overgrowth lamellae structures are similar in morphology to that of the basal lamellae. Both of the structures are spherulitic with radial centrosymmetric in organization. There are two possible arrangements of the basal lamellae and the overgrowth lamellae structures on silicon wafers [Fig. 11]. One of them is an arrangement where the overgrowth structures are formed on top of the basal lamellae (1) and the other is where basal lamellae and the overgrowth structures form side by side on the silicon wafer (2). The second arrangement is highly unlikely because no overgrowth formation is seen in any samples which are not re-crystallized isothermally even in thicker films. But monolayers of basal lamellar spherulites are observed on all the samples. So it can be reasonably concluded that the basal lamellar spherulites are first formed during the re-crystallization process and then overgrowth structures are formed on top of the basal lamellae. Similar conclusions have been also provided by Mareau and Prud'homme [62].

Overgrowth morphology is formed due to secondary heterogeneous nucleation of the excess melt on the surface during isothermal re-crystallization. It is nucleated from surface defects and their growth front is stopped only when neighboring overgrowths impinge on each other. The overgrowth structures with "windmill" crystal morphology is formed only at higher temperatures of re-crystallization as with the decrease of the temperature there would be less nucleation sites for these structures to be formed. Primary nucleation is more dominant with decreasing temperature of $scC0_2$ [63]. Heterogeneous nucleus was presumably too small to give birth to secondary nucleation in annealing process. So overgrowth structure morphology is missing in annealed samples. The structures are quite stable and no changes in morphology have been observed if the samples are kept in air till two weeks.

3.4: Grazing incidence x-ray diffraction (GID) studies of PCL thin and ultrathin films (20-200nm):

GID was performed on the samples to study the lamellar orientation of the crystals; exposed to $scCO_2$ and annealing conditions; after they re-crystallized under the combined effects of

confinement and different degree of supercooling. The incident angle for measurements has been taken as 0.2 degrees which is higher than the critical angle for the bulk polymer. The samples were exposed to x-ray for 300s before the measurements were taken.

3.5: Crystal structure of PCL:

The unit cell of poly-e-caprolactone [Fig. 12] was found to be orthorhombic with dimensions; a = 7.496, b=4.974, c= 17.297 Å (fiber axis), where a, b, c are the lattice parameters of the crystal. The space group is $P2_12_12_1$. This unit cell is only compatible with an extended planar chain conformation of the molecule involving two monomer residues related by a twofold screw axis in the chain direction. Intensity measurements require the rotation of the plane of the chains about their axis to an angle of 28 ° with respect to the axis [64]. Simulation studies have been carried out using unit crystal of PCL.

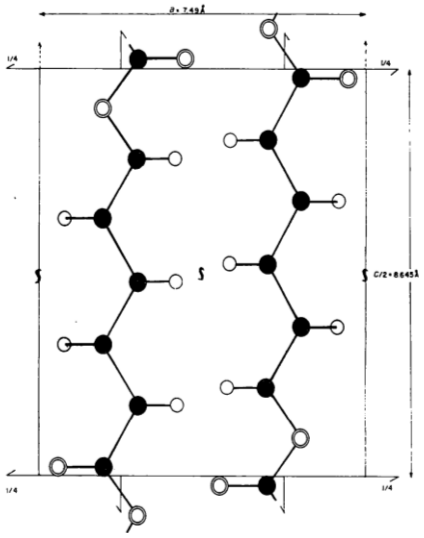

Fig. 12: Unit cell and chain arrangement of PCL in *ac* projection. Only half c/2 of the unit cell is shown in the c direction [49].

3.6: Simulation studies and generated patterns of orientation of lamellae in polymer films:

Computer generated simulation patterns of orientation of lamellae were generated for comparison with actual GID micrographs. Based on the simulation, the orientations of lamellae on actual processed samples are derived. According to simulation patterns, a-axis standing

pattern at an angle of 28˚ with the normal to the plane of substrate is considered as edge-on lamellae and c-axis standing as flat-on lamellae.

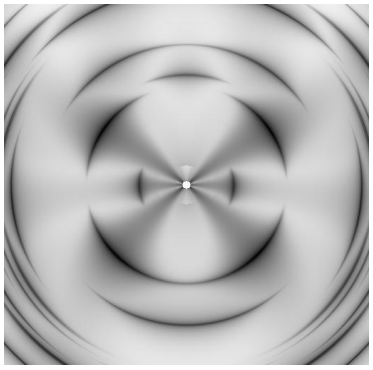

A-axis standing at a tilt of 28 degrees indicates **dge – on orientation** of lamellae in PCL thin films

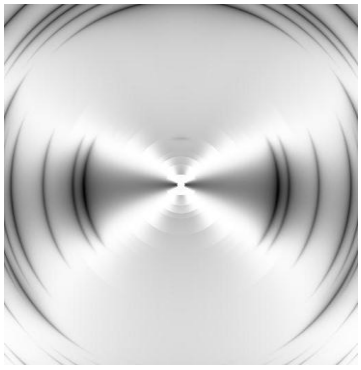

C-axis standing indicates flat –on orientation of lamellae in PCL thin films.

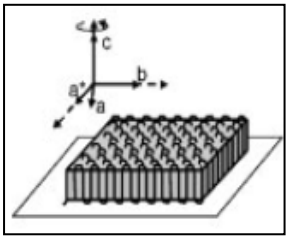

Flat-on lamellar orientation

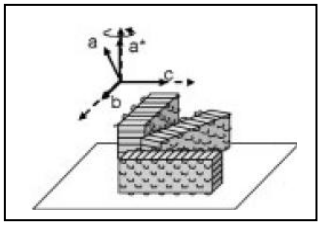

Edge-on lamellar orientation

Fig. 13: Simulation patterns of orientation of lamellae on substrate in case of PCL films.

3.7: Wide angle x-ray diffraction (WAX) studies of bulk PCL polymer at room temperature:

WAX studies of bulk PCL polymer was carried out at room temperature to determine the crystalline structure of the polymer and locate and identify the diffraction peaks in bulk polymer to compare them with the diffraction peaks obtained in GID micrographs of PCL films.

PCL bulk WAX pattern and corresponding graph with 7 visible peaks

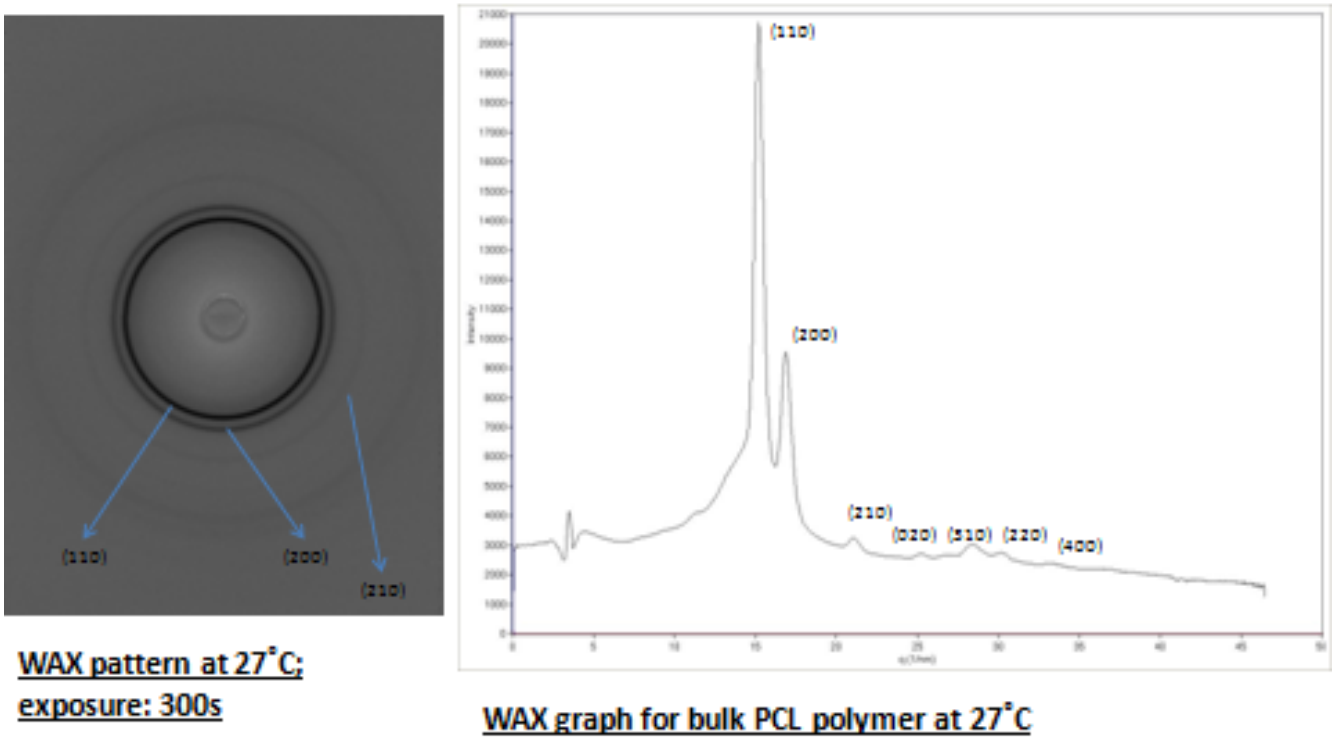

Fig. 14: PCL bulk WAX pattern and corresponding graph showing 7 different visible peaks

Orthorhombic d-spacing formula for calculation of d-spacing and q values from WAX pattern of PCL bulk polymer at room temperature: $\frac{1}{d_{hkl}^2} = \frac{h^2}{a^2} + \frac{k^2}{b^2} + \frac{l^2}{c^2}$; $q = 4\pi\sin\theta/\lambda$;

Where d is crystal lattice spacing in the unit crystal and a, b, c are the lattice parameters of the crystal; h, k, l are the Miller indices of the crystal; 2θ is the diffraction angle and λ is the wavelength of the x-ray.

From the WAX experiments, seven different visible peaks were identified and the observed d-spacing values and q-values were recorded. Using the known lattice parameters for bulk PCL, d-

spacing values and corresponding q values were also calculated for comparison with the experimental values [Table 1].

Observed (h k l)	Observed d (A˚)	Observed q (nm^{-1})	Calculated d (A˚)	Calculated q (nm^{-1})
(110)	4.13	15.194	4.17	15.059
(200)	3.72	16.876	3.748	16.755
(210)	2.97	21.089	2.99	20.96
(020)	2.48	25.256	2.48	25.251
(310)	2.20	28.34	2.23	28.11
(220)	2.08	30.112	2.073	30.29
(400)	1.87	33.444	1.87	33.511

Table 1: Observed d spacing and corresponding q values from the WAX pattern of the bulk polymer and comparison of calculated values using known lattice parameters of PCL and miller indices from the formula.

3.8: Lamellar orientation of PCL crystals on silicon substrate:

To maximize the signal from the thin PCL layer, experiments were conducted at a grazing angle close to the critical angle of the PCL layer (α_i) 0.2° at 11.3 keV). The scattering patterns were recorded using a detector with the X-ray beam parallel to the substrate (i.e., the *x*-axis). The parallel configuration (incident beam nearly parallel to the *x*-axis) gives a Ewald projected pattern approximating the equatorial in-plane scattering [(*hk*0) or, in regard to Figure 6, (*zy*0)]. Fig. 15 shows the in-plane GID profiles of the PCL films. From the micrographs we can see two almost merged strong rings which have been characterized to come from the first order Bragg reflection peak (q= 14.782nm^{-1}) and the second order Bragg reflection peak (q=15.754nm^{-1}). The two strong Bragg reflection peaks have been assigned to (110) plane and (200) plane for 1st and 2nd peaks. These two planes have an angle of 90˚ to a-axis where the c-axis is standing perpendicular to the plane of the substrate with a d-spacing of 0.41 A˚ in between them. The small d-spacing between the planes explain the fact that the two diffraction rings in the GID profiles are almost indistinguishable from each other. The chains are packed regularly together along the c-axis and perpendicular to the substrate axis. All the films, both thin and ultrathin, show flat-on orientation of the lamellae with the lamellae axes parallel to c-axis. The absence of any out-of-plane GIXRD reflection is an additional proof of preferential PCL stem direction perpendicular to the film surface for all different PCL crystallites. GID experiment clearly shows that PCL crystals tend to align themselves in a flat-on orientation to the substrate when re-

crystallized after $scCO_2$ processing or conventional annealing process. The flat-on orientation is prevalent in all samples for both low and high degrees of supercooling and confinement effects from 20-200nm.

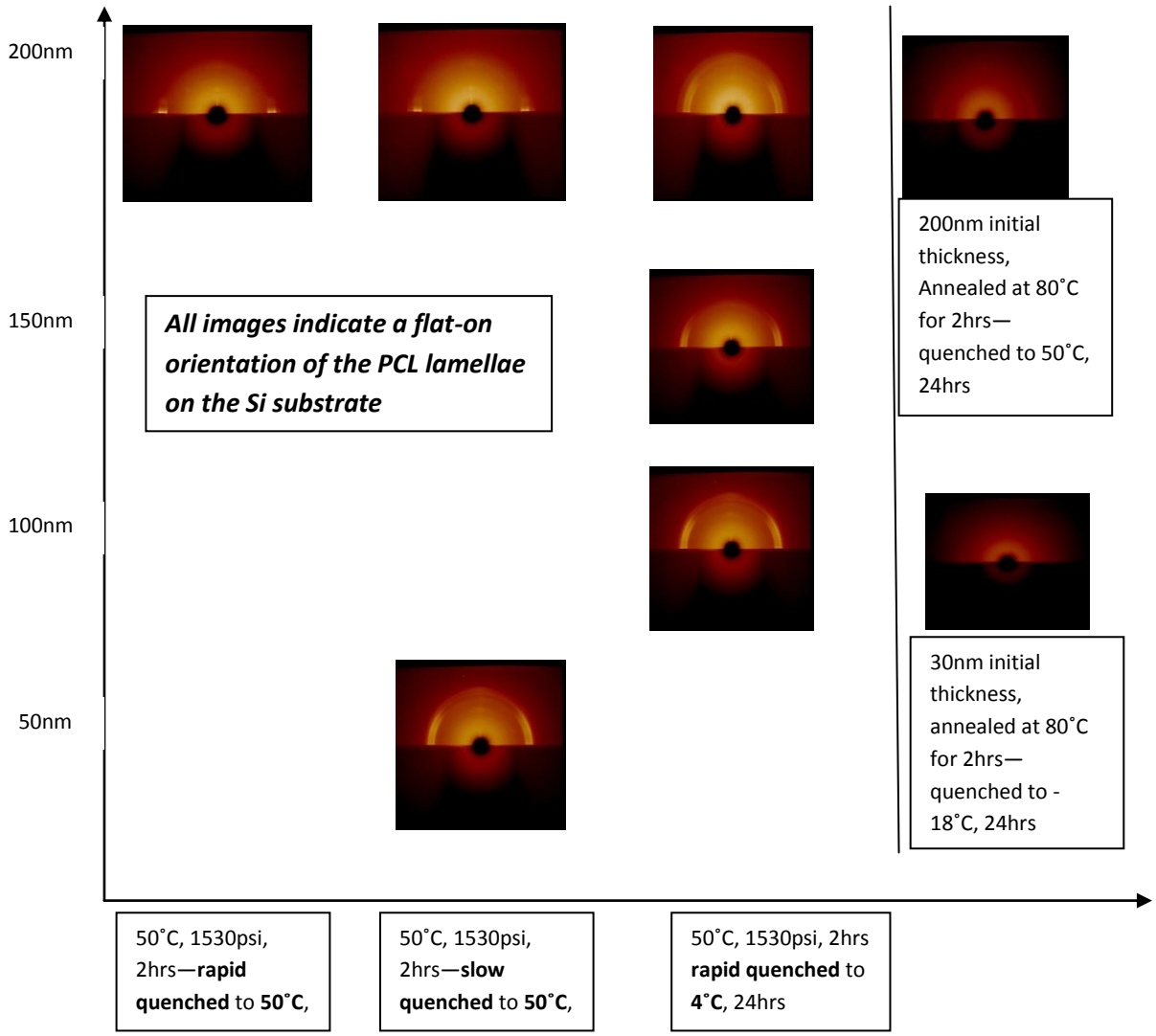

Fig. 15: GID profiles of PCL films processed under effects of confinement and supercooling nearly parallel to the *x*-axis

Fig. 16 shows the GID profile for the same initial thickness of 100nm for two different methods of re-crystallization process. One sample was annealed at 80˚C for 2 hrs and quenched to -18˚C and kept isothermally for 1 day and the other processed in $scCO_2$ at ridge condition and rapidly quenched to 4˚C and isothermally kept for 1 day. The $scCO_2$ processed sample shows clearly two Bragg diffraction peaks while the annealed sample has very faint peaks although the annealed sample has been re-crystallized at a much lower temperature. It may be because the $scCO_2$ processed sample is much closer to the reported glass transition temperature, and this increased intensity likely originates from the process of "cold crystallization" and improved ordering within crystal domains which is likely suppressed even at much lower temperatures in annealing process. Super critical CO_2 processing at ridge condition acts as a good plasticizer for PCL thereby reducing the glass transition temperature; adding to higher mobility of polymer chains and thereby enabling them to rearrange the chains in improved ordered state. At slow quench process (Fig. 17) and with increasing film thickness (Fig. 20), scattering peak drops in intensity. Two factors likely contribute to this effect: first is the drop due to thermal motion, and second is the occurrence of a broad transition from the melt to crystalline phase during re-crystallization. It is clearly observed that $scCO_2$ processing of the samples near the critical point (T=31.3˚C and P=7.38˚C) with rapidly quenching of the samples shows improved crystal size and crystalline ordering compared to other $scCO_2$ and conventional high temperature annealing processes.

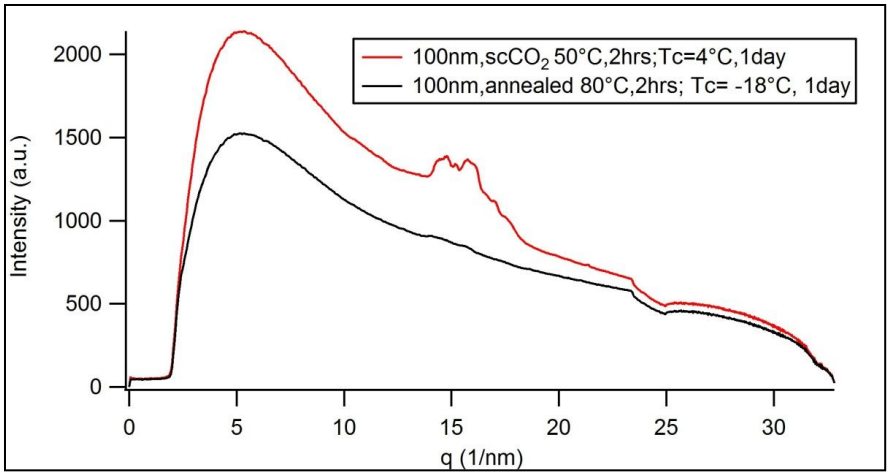

Fig. 16: GID profiles of PCL film of 100nm initial thickness processed in $scCO_2$ at 50˚C for 2 hrs and rapid quenched to Tc=4˚C for 1 day and same thickness film annealed at 80˚C for 2 hrs and quenched to TC=-18˚C for 1 day

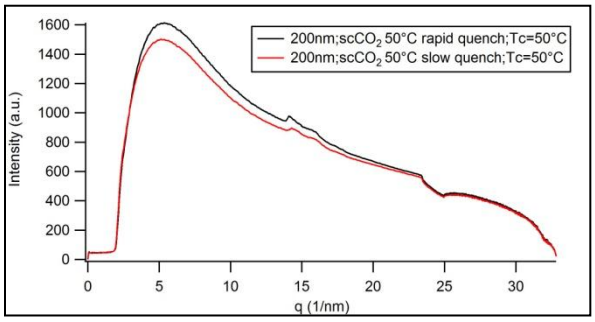

Fig. 17: GID profiles of PCL film of 200nm initial thickness processed in $scCO_2$ at 50˚C for 2 hrs and rapid quenched and slow quenched to Tc=50˚C for 1 day

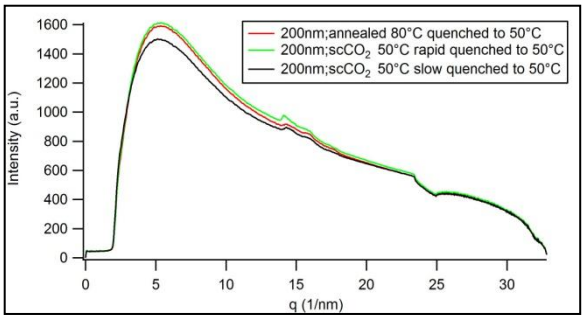

Fig. 18: GID profiles of PCL film of 200nm initial thickness processed in $scCO_2$ at 50˚C for 2 hrs and rapid quenched ; slow quenched and annealed to 80˚C for 2hrs and quenched to 50˚C for 1 day

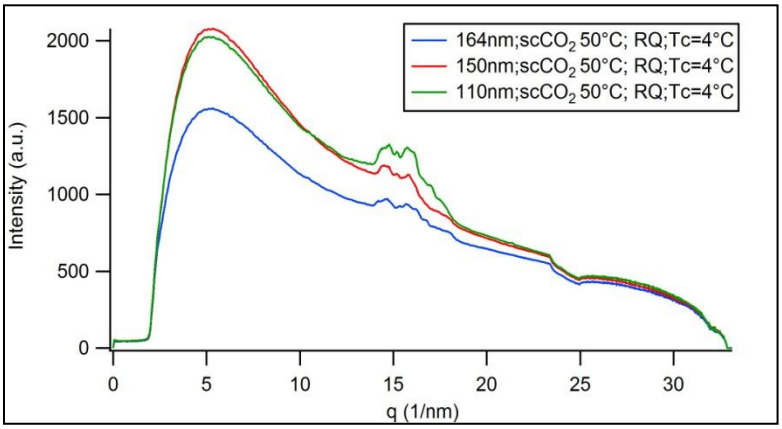

Fig. 19: GID profiles of PCL film of different initial thickness processed in $scCO_2$ at 50˚C for 2 hrs and rapid quenched to Tc=4˚C for 1 day

3.9: GISAXS profiles of PCL ultrathin films processed with supercritical carbon dioxide:

Grazing-Incidence Small-Angle X-ray Scattering (GISAXS) is a versatile tool for characterizing nanoscale density correlations and/or the shape of nanoscopic objects at surfaces, at buried interfaces, or in thin films. GISAXS of PCL ultrathin films were performed at Brookhaven National Laboratory to find out the orientation of the monolayer of polymer on the substrate. The wavelength (λ) used for the experiments is 0.1093 nm. The incident angle (α_i) for the GISAXS experiments has been chosen as 0.2˚. The critical angle ($\theta_c = \lambda(\rho_e\, r_e/\pi)$) is directly related to the average electron density (ρ_e) in a film, and the total thickness of a film is extracted from the oscillation frequency of a uniform mode. The incident angle (α_i) chosen here is less than critical angle for silicon, $\theta_{c\,(Si)}$, which is equal to 0.22 but greater than the average critical angle for the polymer. The GISAXS profiles give an average orientation of the monolayer of polymer on the substrate. A few of the GISAXS profiles along the q_z direction for the ultrathin films are shown in Fig. 21.

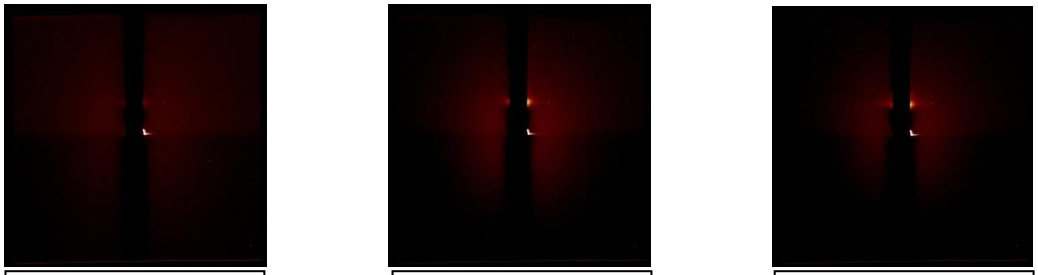

20 nm initial thickness, 50˚C, 1530psi, 2hrs—**rapid quenched** to **ambient pressure and temperature**

50 nm initial thickness, 50˚C, 1530psi, 2hrs—**rapid quenched** to **ambient pressure and temperature**

100 nm initial thickness, 50˚C, 1530psi, 2hrs—**rapid quenched** to **ambient pressure and temperature**

Fig. 20: GISAXS profiles of obtained from the transformation along the reflected beam for various thickness of PCL films exposed to $scCO_2$ exposure for 2 hrs at 50C and 1530psi pressure inside a chamber and subsequent quenching to ambient pressure and temperature. The α_i = 0.2 and the exposure time = 300 s.

The GISAXS profiles clearly show that the polymer strongly favors the substrate, the lamellae is parallel to the substrate. The signature of parallel lamellae in GISAXS is stripes of intensity at regular spacing along the q_z direction which is observed in the GISAXS profiles which further solidify the argument that the lamellae are arranged in a flat-on orientation over the Si substrate.

3.10: Effect of substrate on the lamellar orientation in PCL films:

The preferential lamellar orientation of flat-on lamellae of PCL in thin and ultrathin films can be explained on the basis of interfacial interactions of PCL polymer with Si substrate. The affinity between the liquid and solid substrate can be determined on the basis of the interfacial energy γ_{sl} calculated using Owens-Wendt-Kaelble equation:

$$\gamma_{sl} = \gamma_l + \gamma_s - 2(\gamma_s^d \gamma_l^d)^{1/2} - 2(\gamma_s^p \gamma_l^p)^{1/2}$$

in which γ_s^d and γ_s^p are the dispersion and polar parts of the surface energy of the solid phase and γ_l^d and γ_l^p are the dispersion and polar parts of the surface energy of the liquid phase.

Since in all of the crystallization processes carried out, PCL has been heated to a temperature greater than the melting temperature of the bulk polymer, so it can be taken as the liquid phase and silicon can be taken as the solid phase. The γ_s^d and γ_s^p for silicon is 48.71mJ/m^2 and 3.98mJ/m^2 and γ_l^d and γ_l^p for PCL is 41mJ/m^2 and 11mJ/m^2 respectively.

Calculating the interfacial energy between PCL and silicon, we get $\gamma_{Si/PCL}$ = 1.09mJ/m^2.

The value for interfacial energy between a similar semicrystalline polymer PEO and silicon is 4.18mJ/m^2.

So the interaction between silicon and PCL is very strong which results in strong depression of both crystallization rate and final crystallinity due to restriction of polymer motions within the contact layers. This flat-on lamellae orientation is a result of heterogeneous nucleation of the crystalline structure from the melt. It is shown earlier that initially edge-on and flat-on lamellae grow simultaneously at the same rate during the re-crystallization process but due to strong interactions between the polymer and the substrate the lateral growth of edge-on crystals is almost completely suppressed and even the flat-on lamellae growth is much slower. Edge-on lamellae growth starts at the polymer-air interface for films and the flat-on lamellae growth from

the polymer-substrate interface. But due to strong interaction of the polymer-substrate interface in case of PCL films on silicon substrate, edge–on lamellae orientation is quickly overcome by flat-on lamellae growth front from the polymer-substrate interface at least up to 200nm of film thickness measured in experiments. Fig.22 shows a model of the effect of substrate interfacial energies on the lamellar orientation of the polymer during re-crystallization process. In case of slippery walls where the polymer-substrate interaction is weak, slippery walls show weak enhancement of crystallization for thin films. Slippery walls reflect neutral repulsion of polymer thus assisting in surface assisted crystal nucleation forming dominant edge-on lamellae. In case of sticky walls where the polymer-substrate interaction is strong, sticky walls show significant depression of crystallization for thin films. Sticky walls arrest the movement of polymers in contact with the substrate thus forming preferential flat-on lamellae.

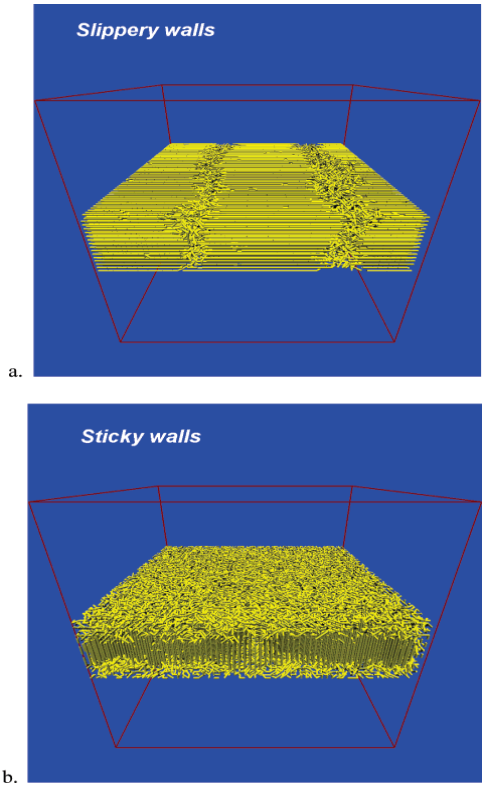

a.

b.

Edge-on lamellae in this case in 1D confinement

Flat-on lamellae in this case in 1D confinement

Fig. 21: Effect of substrate on the lamellar orientation of polymer in 1D confinement. Slippery walls are substrates where polymer-substrate interaction is weak (edge-on lamellae) and sticky walls are substrates where polymer-substrate interaction is strong (Flat-on lamellae). [65].

3.11: Effect of temperature of crystallization during the quenching process:

It is well known that as thin or ultrathin films are quenched to temperatures closer to the glass transition temperature of the polymer, a transition from preferential flat-on lamellae to edge-on lamellae is expected to seen. The glass transition temperature of PCL is ~ -60^{o}C. Experiments on thin and ultrathin films have carried out from temperature of crystallization of 50^{o}C through 4^{o}C in supercritical carbon dioxide and conventional annealing in vacuum and quenching in air from 50^{o}C through -18^{o}C. In this temperature range we can only see flat-on orientation of lamellae in all samples which is indifferent of the process or supercritical carbon dioxide or conventional annealing. Moreover the rate of quenching (rapid or slow [-1psi/sec to atm pressure]) in case of super critical carbon dioxide does not affect the lamellar orientation in both thin and ultrathin films.

Chapter 4: Conclusions and future work

The effect of supercritical carbon dioxide on the crystallization behavior of PCL in ultrathin and thin films has been investigated. Moreover the effects of supercooling and confinement on the crystallization behavior of polymer on the same films have also been studied. The effects of a novel plasticizer like supercritical carbon dioxide with conventional process of annealing on the crystallization behavior of PCL polymer on thin and ultrathin films using various techniques like polarized optical microscopy, AFM, GISAXS, and GID have been compared.

The studies show that overgrowth morphology is formed due to secondary heterogeneous nucleation of the excess melt on the surface during isothermal re-crystallization in samples processed in supercritical carbon dioxide. It is nucleated from surface defects and their growth front is stopped only when neighboring overgrowths impinge on each other. Heterogeneous nucleation is presumably too small to give birth to secondary nucleation in annealing process. So overgrowth structure morphology is missing in annealed samples. The size of the overgrowth structures decreases with the decrease of film thickness in case of $scCO_2$ processed samples. The structures are quite stable and no changes in morphology have been observed if the samples are kept in air till two weeks. In case of PCL films the basal lamellae spherulite size decreases with the increase in the supercooling and at thickness comparable to 5Rg of the polymer, polymer can no longer form big spherulites and tend to crystallize in small pockets forming a hill-valley structure.

GID experiments clearly show that PCL polymer tend to arrange in flat-on lamellar orientation on silicon substrate when re-crystallized after $scCO_2$ processing or conventional annealing process. The flat-on orientation is prevalent in all samples irrespective of low and high degrees of supercooling and confinement effects. The results indicate that $scCO_2$ processing at ridge condition can induce much larger ordering of crystals at a lower degree of supercooling than conventional annealing processing at higher degree of supercooling. So it can be reasonably concluded that $scCO_2$ processing enhances the crystallization process. It is also seen that rapid quenching process during re-crystallization in $scCO_2$ processed samples produce a higher ordering of crystals in PCL samples than slow quenching process. The flat-on lamellar orientation of PCL polymer on the silicon substrate is due to very strong interactions between the polymer and the substrate causing significant depression of crystallization for thin films. This

arrests the movement of polymers in contact with the substrate thus forming preferential flat-on lamellae.

The present experiments have confirmed that the crystallization of PCL on silicon substrate is dominated by lamellae growth from polymer-substrate interface forming thereby preferential flat-on lamellar orientation. Recently our group has published the role of the irreversibly adsorbed layer of polymer on local viscosity in nanoconfined melts [66]. Future experiments will be carried out to understand the role of irreversibly adsorbed layer of ~3nm of PCL polymer on the re-crystallization behavior of PCL in thin and ultrathin films.

References:

[1]. R. Chandra, R. Rustgi, Prog. Polym. Sci., Jpn. 1998, 23, 1273

[2] http://www.sigmaaldrich.com/catalog/product/aldrich/704105?lang=en&region=US, http://www.biodeg.net/bioplastic.html

[3] C.W. Frank, V. Rao, M.M. Despotopoulou, R.F.W. Pease, W.D. Hinsberg, R.D. Miller, J.F. Rabolt, Science 273 (1996) 912.

[4] Yi-Xin Liu et al. Coordination chemistry reviews 254 (2010) 1011-1037

[5] S.Z.D. Cheng, Phase Transitions in Polymers: The Role of Metastable States, Elsevier, Amsterdam, 2008.

[6] K. Armitstead, G. Goldbeck-Wood, Adv. Polym. Sci. 100 (1992) 219.

[7] H. Schönherr, C.W. Frank, Macromolecules 36 (2003) 1188.

[8] H. Schönherr, C.W. Frank, Macromolecules 36 (2003) 1199.

[9] S. Napolitano, M. Wübbenhorst, J. Phys. Chem. B 111 (2007) 5775.

[10] S. Napolitano, M. Wübbenhorst, Macromolecules 39 (2006) 5967.

[11] S. Napolitano, M. Wübbenhorst, J. Phys. Conds. Matter. 19 (2007) 205121.

[12] J.M. Schultz, Macromolecules 29 (1996) 3022.

[13] A. Keller, G. Goldbeck-Wood, in: Aggarwal, Russo (Eds.), Comprehensive Polymer Science: 2nd Supplement, Elsevier, Oxford, 1996, p. 241.

[14] Y. Jiang, D. Yan, X. Gao, C.C. Han, X. Jin, L. Li, Y. Wang, C. Chan, Macromolecules, 36 (2003) 3652.

[15] V.H. Mareau, R.E. Prud'homme, Macromolecules 38 (2005) 398.

[16] http://www.dur.ac.uk/sharon.cooper/lectures/cryskinetics/handoutsalla.html

[17] Ellison CJ, Torkelson JM. Nat Mater 2003; 2:695.

[18] Priestley RD, Ellison CJ, Broadbelt LJ, Torkelson JM. Science 2005; 309:456.

[19] Padden FJ, Keith HD. J Appl Phys 1966; 37:4013.

[20] Basire C, Ivanov DA. Phys Rev Lett 2000; 85:5587.

[21] Muratoglu OK, Argon AS, Cohen RE. Polymer 1995; 36:2143.

[22] Wang Y, Ge S, Rafailovich M, Sokolov J, Zou Y, Ade H, et al. Macromolecules 2004;37:3319.

[23] Lovinger AJ, Keith HD. Macromolecules 1979;12:919.

[24] Kovacs AJ, Straupe C. Faraday Discuss 1979;68:225.

[25] Schonherr H, Frank CW. Macromolecules 2003;36:1188.
[26] Wittmann JC, Lotz BJ. Polym Sci Polym Phys Ed 1985;23:205.
[27] Keith HD, Padden FJ, Lotz B, Wittmann JC. Macromolecules 1989;22:2230.
[28] Bu Z, Yoon Y, Ho ReM, Zhou W, Jangchud I, Eby RK, et al. Macromolecules 1996;29:6575.
[29] Sutton SJ, Izumi K, Miyaji H, Miyamoto Y, Miyashita S. J Mater Sci 1997;32: 5621.
[30] Abe H, Kikkawa Y, Iwata T, Aoki H, Akehata T, Doi Y. Polymer 2000;41:867.
[31] Hu ZJ, Huang HY, Zhang FJ, Du BY, He TB. Langmuir 2004;20:3271.
[32] Sakai Y, Imai M, Kaji K, Tsuji M. Macromolecules 1996;29:8830.
[33] Mareau VH, Prudhomme RE. Macromolecules 2005;38:398.

[34] Taguchi K, Miyaji H, Izumi K, Hoshimo A, Miyamoto Y, Kokawa R. Polymer 2001;42:7443.
[35] Theodorou DN. Macromolecules 1989;22:4578.
[36] Mansfield KF, Theodorou DN. Macromolecules 1991;24:4295.
[37] Mansfield KF, Theodorou DN. Macromolecules 1990;23:4430.
[38] Harmandaris VA, Kaoulas KC, Mavrantzas VG. Macromolecules 2005;38:5796.
[39] Ma Y, Hu W, Reiter G. Macromolecules 2006; 39: 5159.
[40] Wang Y, Chan CM, Ng KM, Li L. Macromolecules 2008; 41: 2548.
[41] Qiao C. et al. Journal of Polymer Science: Part B: Polymer Physics, Vol 43, 1303-1309 (2005).
[42] Mareau et al. Macromolecules, 2005, 38, 398-408.
[43] Davis GT, Eby RK, Martin GM. Journal of Applied Physics 1968;39 (11):4973–81.
[44] Leisen J, Beckham HW, Sharaf MA. Macromolecules 2004;37(21):8028–34.
[45] Pitt, C. G. In *Biodegradable Polymers as Drug Delivery Systems*; Chasin, M., Langer, R., Eds.; Marcel Dekker: New York, 1990; pp 71-120.
[46] Ciapetti, G.; Ambrosio, L.; Savarino, L.; Granchi, D.; Cenni, E.; Baldini, N.; Pagani, S.; Guizzardi, S.; Causa, F.; Giunti, A. *Biomaterials* **2003**, *24*, 2815.
[47] Massa, M. V.; Dalnoki-Veress, K.; Forrest, J. A. *Eur. Phys. J.* **2003**, *11*, 191.
[48] Mareau, V. H.; Prud'homme, R. E. *Macromolecules* **2002**, *36*, 675.

[49] Bittiger, H.; Marchessault, R. H. *Acta Crystallogr*. **1970**, *B26*, 1923.

[50] AFPO Group, Laboratory of Solid State Physics, Ellipsometry, CNRS & Universite Paris.

[51] R. M. A. Azzam and N.M. Bashara, Ellipsometry and Polarized Light, Elsevier Science Pub Co, ISBN 0-444-87016-4, 1987

[52] A. Roeseler, Infrared Spectroscopic Ellipsometry, Akademie-Verlag, bErlin, ISBN 3-05-500623-2, 1990.

[53] http://en.wikipedia.org/wiki/Ellipsometry.

[54] Koga, T.; Seo, Y. S.; Shin, K.; Zhang, Y.; Rafailovich, M. H.; Sokolov, J. C.; Chu, B.; Satija, S. K. Macromolecules 2003, 36, (14), 5236-5243.

[55] Moonhor Ree et al, Macromolecules 2005.

[56] Findenegg, G. H., In Fundamentals of Adsorption; Myers, A. L.; Belfort, G., Eds.; Engineering Foundation: New York, 1984, p 207.

[57] Strubinger, J. R.; Song, H.; Parcher, J. F. Anal Chem 1991, 63, 98.

[58] Strubinger, J. R.; Parcher, J. F. Anal Chem 1989, 61, 951.

[59] Koga, T.; Seo, Y. S.; Shin, K.; Zhang, Y.; Rafailovich, M. H.; Sokolov, J. C.; Chu, B.; Satija, S. K. Macromolecules 2003, 36, 5236.

[60] Sergei G. Kazarian et al. J. Am. Chem. Soc. 1996**,** 118, 1729-1736.

[61] S. H. Murphy • G. A. Leeke • M. J. Jenkins, J Therm Anal Calorim, (2012), 107:669–674.

[62] Mareau and Prud'homme, Macromolecules, 38, 2005, 398-408.

[63] Jie Wang et al. Macromolecules 2001, 41, 1273-1280.

[64] Bittiger et al. Acta Cryst. (1970). B26, 1923.

[65] Yu Ma et al. Macromolecules 2006, 39, 5159-5164.

[66] T. Koga et al. Physical Review Letters, 107, 225901, 2011.